Citation
Wang, C. and Chen, W. and Hao, H. and Zhang, S. and Song, R. and Wang, X. 2018. Experimental investigations of dynamic compressive properties of roller compacted concrete (RCC). Construction and Building Materials. 168: pp. 671-682. http://doi.org/10.1016/j.conbuildmat.2018.02.112

Experimental investigations of dynamic compressive properties of roller compacted concrete (RCC)

Chao WANG [a,b,c], Wensu CHEN[c], Hong HAO [c], Sherong ZHANG [a,b], Ran SONG [a,b], Xiaohua WANG [a,b]

([a] State Key Laboratory of Hydraulic Engineering Simulation and Safety, Tianjin University, Tianjin 300072, China,

[b] School of Civil Engineering, Tianjin University, Tianjin 300072, China,

[c] Centre for Infrastructural Monitoring and Protection, School of Civil and Mechanical Engineering, Curtin University, Kent Street, Bentley, WA 6102, Australia)

Abstract: Roller compacted concrete (RCC) has been widely used in large scale constructions such as hydraulic structures and pavement. Because of the construction process, it has some unique material properties as compared to the ready-mix concrete. Structures made of RCC might be subjected to dynamic loads during its service life. Understanding the dynamic material properties of RCC is essential for better analysis and design of RCC structures. The study on dynamic compressive mechanical properties of RCC is very limited in literature. In this study, dynamic compressive properties of RCC under the strain rate up to 80 /s are investigated by using Split Hopkinson Pressure Bar (SHPB). In addition, to investigate the size effects on dynamic impact tests, three sizes of cylindrical RCC specimens with the diameters of 50 mm, 75 mm and 100 mm are prepared and tested. The failure processes and the failure modes of RCC specimens with different dimensions under different strain rates, as well as the stress–strain curves under different strain rates and the energy absorption capacities of the tested specimens are compared. The influences of the specimen size, aggregates grading, and the existence of bedding surface in RCC on its dynamic properties are investigated. Based on the testing results, empirical formulae of DIF (dynamic increase factor) for the RCC compressive strength are proposed to predict the enhancement of material strength at different strain rates.

Keywords: Roller compacted concrete (RCC); Bedding surface effects; Strain rate effect; Compressive strength; SHPB

Highlights:

- Dynamic stress–strain curves and failure modes of RCC specimens under different strain rates are obtained.
- Empirical relations of DIF of compressive strength for RCC are proposed.
- Influences of aggregate size and lateral inertia confinement on RCC dynamic strength enhancement are studied.
- The effect of bedding surface on the dynamic strength of RCC is examined.

1. Introduction

Roller Compacted Concrete (RCC) material has been widely applied in the constructions of infrastructure such as hydraulic structures and pavement [1-3] due to its advantages of cost-effectiveness and rapid construction. RCC, as a special type of concrete material, has different mixture from traditional concrete, for example using less water and more fly ash to replace Portland cement. The RCC mixture is paved and spread by using bulldozer and then compacted to a layered structure by using vibratory roller. RCC has been utilized for construction of large structures such as dams and airport pavement. During the service life, these structures may be subjected to different types of loads such as blast and impact loads. Therefore, it is necessary to understand the dynamic mechanical properties of RCC materials. Besides, RCC has bedding surfaces [4-6]. The existence of the bedding surfaces and micro-cracks at the interfaces and transition layers affect the mechanical properties of the layered RCC. The effects of bedding surface on dynamic compressive behavior of RCC material therefore also need be investigated.

Dynamic compressive behaviors of concrete and concrete-like material under intermediate-high strain rates have been studied [7-11]. Under dynamic loadings, the evolution of micro-cracks and micro-pores is constrained due to water viscosity effect and micro-inertial effect [12-14]. The difference of concrete behaviors under static and dynamic loadings is caused by strain rate effects. The strain rate effect on concrete material properties has been intensively studied since 1990’s [15, 16]. Aoyama and Noguchi [17] presented a detailed review on the strain rate effects on concrete properties. The descriptions about strain rate effects are summarized as viscosity effect (also called as Stefan effect) [13, 18, 19], evolution of cracks [20-22] and inertial effect [7, 23]. The influence of strain rate on concrete properties including dynamic strength, fracture strain and Young’ modulus has been studied. It has been reported that the shape, grading and content of coarse aggregate can affect mechanical properties of concrete under high strain rate. The effect of coarse aggregates on the dynamic tensile strength of concrete has been investigated [24]. The effect of coarse aggregates on the dynamic compression strength has also been investigated and quantified [22]. Hao et al. summarized the influence factors on concrete dynamic strength[25]. It is found that compressive behaviors of cement-based materials are sensitive to strain rate [26] and the strength enhancement at various strain rates is usually represented by the dynamic increase factor (*DIF*), which is defined as the ratio of the dynamic strength to the quasi-static strength of the material. The available empirical DIF formulae on concrete compressive strength include CEB recommendation [27], Tedesco and Ross's model [28], Grote's model [9], Katayama's model [29] and Hao's model[30]. Strain rate effects of normal weight concrete after exposure to elevated temperature are also experimentally investigated and the corresponding DIFs are proposed[31]. Hao et al. [7] experimentally investigated the influences of lateral inertia confinement, end friction confinement and aggregates in SHPB tests on dynamic compressive properties of concrete. In addition, dynamic compressive behavior of new kinds of concrete and concrete-like materials have been studied recently [11, 32]. An experimental investigation on the dynamic mechanical properties of the reactive powder concrete (RPC) was conducted using the split-Hopkinson pressure bar (SHPB) [33]. The compressive behaviour of recycled aggregate concrete (RAC) with different recycled coarse aggregate (RCA) replacement percentages was experimentally investigated under quasi-static to high strain rates[34]. RCC has the same basic ingredient as conventional concrete, but unlike conventional concrete, it is a drier mix with different mixture so that it is stiff enough to be compacted. Therefore RCC has different mechanical properties from the conventional concrete. The existing study about RCC in literature paid more attention to the efficacy of compaction and the quasi-static material properties [35-37]. The study of dynamic compressive behavior and failure mechanism of RCC is very limited [38, 39].

In this study, the dynamic compressive tests of RCC are carried out by using Split Hopkinson Pressure Bar (SHPB) to investigate its compressive properties and strain rate dependent behavior. A total of 54 specimens with the same L/D ratio (specimen length to diameter ratio) of 0.5, but different diameters, i.e. 50 mm, 75 mm and 100 mm are prepared and tested. The dynamic mechanical behaviors in terms of failure pattern, compressive strength and energy absorption capacities are obtained from the tests. The stress-strain curves and dynamic increase factors (DIF) of the strength and the energy absorption capacities are analyzed and compared. The influencing factors including specimen size, aggregate grading and the existence of bedding surface of RCC on the compressive strength of RCC specimens are studied. Empirical formulae of the compressive strength DIF of RCC are proposed to predict the enhancement of compressive strength at different strain rates.

2 Characteristics of RCC

RCC made of concrete mixture is paved and compacted into thin layers by using layered rolling technique. It has the following specific characteristics [40]. Its mixture is composed of low cement content, fly ash, water reducer and air entraining agent, mixed with different sizes of aggregates. RCC mixture is easy to be transported and constructed without longitudinal joint. The mechanical properties of RCC are affected by the macro-structure, composition, aggregate and cement characteristics. Typical layered structure of RCC consists of two components, i.e. the bedding surface and the noumenon layer. Bedding surfaces also named as effect zones appearing between layers during the rolling process. Fig. 1 shows the layered structure of RCC and the bedding surface, where *B and* b_a represent the thickness of each RCC layer and bedding surface, respectively. B-b_a denotes the thickness of RCC noumenon layer. As reported in the previous studies [40-42], the thickness of the bedding surface (b_a) is 0.5~2cm, which accounts for 1.7%~6.7% of the total thickness of an RCC layer.

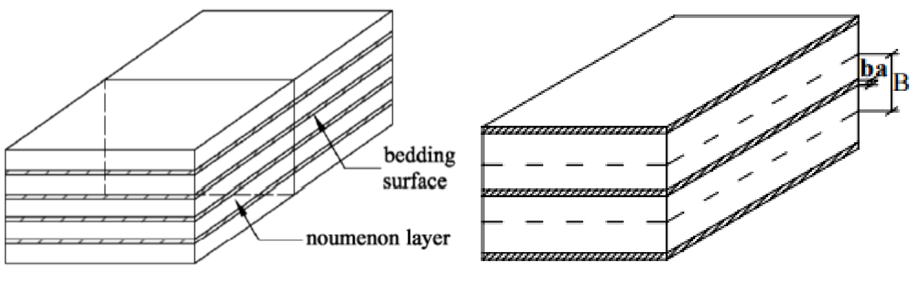

(a) (b)

Fig.1 Schematic diagram of layered RCC. (a) Layered structure of RCC (bedding surface; noumenon layer), (b) Bedding surface model [40]

3. **Experimental program**

3.1 Mixture of specimens

The RCC mixture is made of mortar matrix, aggregates and additive. The mortar matrix is a mixture of water, cement, sand, fly ash, water reducing agent and air-entraining agent. The water-cement ratio (W/C) is set as 0.50. The fly ash content and the sand ratio is 60% and 31% by weight, respectively. The normal Portland cement (NPC) with surface area of 325 m^2/kg and CaO content of 62.97% is used in the mixture. The details of the RCC mixture are given in Table 1. Two types of aggregate grading (Ⅰ and Ⅱ) are prepared as given in Table 2. The maximum size of the coarse aggregate is 15 mm to satisfy the requirement of sample size for SHPB test.

Table 1. Mixture and material properties of RCC

W/C	Sand ratio (%)	Fly ash content (%)	Water reducing agent (%)	Air entraining agent (%)	Material consumption（kg/m^3）					Air content (%)	Wet density (kg/m^3)
					Water	Cement	Fly ash	Sand	Aggregate		
0.50	31	60	0.8	0.05	88	70	106	672	1507	3.8	2453

Note: W/C: water to cement ratio

Table 2. The composition of coarse aggregate size

Aggregate grading	Large aggregate size (mm)	Medium aggregate size (mm)	Small aggregate size (mm)	Composition (%) by weight
I	10	5～10	5	40:30:30
II	15	10～15	5～10	40:30:30

3.2 Specimen preparation

The preparation processes of specimens are given below. RCC mixtures were prepared before paving with the V_C index of 3.7s indicating workability. Heavy duty mechanical tamper with the frequency of 50 Hz~70 Hz was then used to vibrate and compact RCC mixtures, as shown in Fig.2 (a). Rolling technique following “two static rolling + eight dynamic rolling + two static rolling” was adopted for layer compaction. Each layer was compacted to the paving thickness of 10 cm. After 90 days curing, drilling tubes with different diameters (i.e. Ø50mm, Ø75mm, and Ø100mm) were used to core the samples with different sizes. As shown in Fig.2 (b-d), the cored samples were cut and grinded at both ends to ensure that the surfaces are parallel. The roughness of the surfaces is less than 0.02 mm, which is believed that the error in transmitting stress wave due to the non-perfect contact can be negligible. In this study, 54 specimens with the same L/D ratio of 0.5, but different diameters, i.e. 50 mm, 75 mm and 100 mm were prepared and tested. Owing to the nature of RCC material, bedding surfaces existed in the cored samples. When the cored samples were cut into the specimens for SHPB test, some specimens had one bedding surface while others had no bedding surface as shown in Fig.3. Among them, there were 18 specimens with bedding surface and 36 specimens without bedding surface. In addition, six specimens (the size of Ø100–200 mm) with the two aggregate grading were prepared for quasi-static compressive tests and the quasi-static compressive strength was employed to calculate the DIF of compressive strength [43].

(a) (b) (c) (d)

Fig. 2 Specimen preparation for SHPB tests. (a) Compaction of RCC, (b) Sample coring, (c) RCC cores, (d) Ø100-50mm specimens for SHPB test

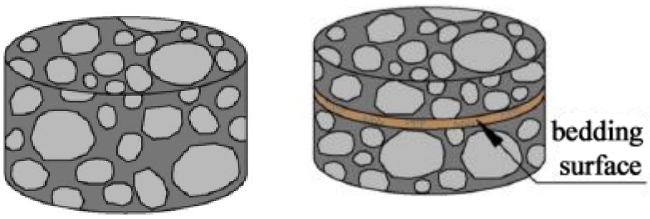

(a) (b)

Fig. 3 Schematic diagrams of specimens without or with bedding surface. (a) Specimen without bedding surface;

(b) Specimen with bedding surface

3.3 SHPB test apparatus

Dynamic material tests were conducted by using SHPB test system. As shown in Fig. 4, both incident and transmitted bars have the length of 2000 mm with the diameter of 100 mm and the absorption bar is 1000 mm long with the diameter of 100 mm. A loading chamber is connected with a nitrogen tank and two valves (i.e. Valve A and Valve B) are instrumented. Valve A is connected to the nitrogen tank and Valve B is used to accumulate and release pressure in the chamber. The detailed loading procedures are given in literature [44]. The relationships between stress, strain, strain rate and time can be determined by two-wave formulae [9].

A tapered impact ram [45] was used as the striker bar for the testing of concrete-like material. By using such a projectile, a half-sine loading waveform was generated to mitigate violent oscillation and dispersion. Grease was applied at the specimen–bar interfaces to minimize the influence of end friction confinement [46]. Pulse shaping method is used by mounting a pulse shaper on the impact end of incident bar to obtain half-sine-like stress wave. The use of pulse shaper [47] also prolongs the rising time of incident pulse, which makes it easier to achieve stress equilibrium and constant strain rate.

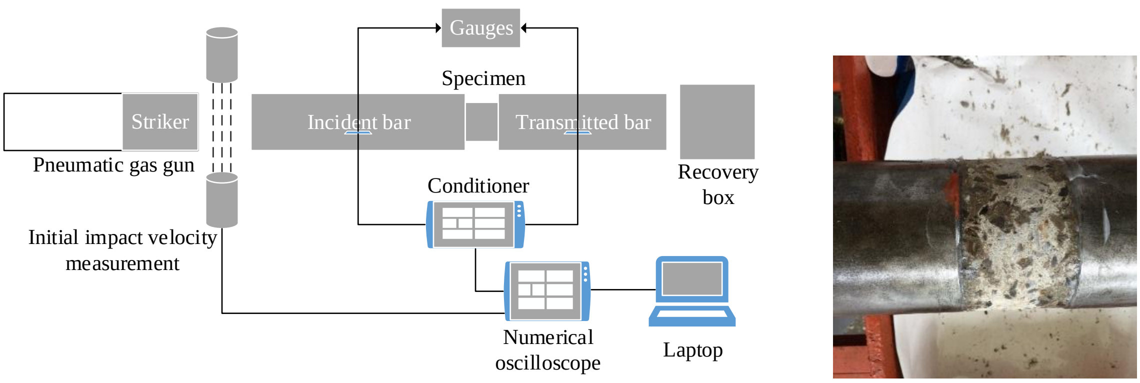

(a) (b)

Fig. 4 SHPB test system (a) Schematic diagram of SHPB test system, (b) Specimen

4. Testing results and discussions

4.1 Quasi-static test results

Quasi-static compressive tests on the Ø100-200mm specimens were conducted by using an electro-hydraulic servo-controlled loading test machine at Tianjin University. The testing machine delivers a constant crosshead movement with the loading rate of 1.20 mm/min, corresponding to a quasi-static strain rate of 1×10^{-4}/s. The 90-day uniaxial compressive strength, Young's modulus and critical strain of RCC with aggregate grading Ⅰ were measured as 11.55 MPa, 2.68 GPa and 0.76%, respectively. The corresponding values of RCC with aggregate grading Ⅱ were measured as 10.17 MPa, 2.64 GPa and 0.71%, respectively.

4.2 Determination of strain rate

Based on the theory of one-dimensional stress wave propagation, the strain (ε), strain rate ($\dot{\varepsilon}$) and stress (σ) of the specimen can be obtained from the measured reflected wave (ε_R) and transmitted wave (ε_T) by using the following formulae[48].

$$\sigma(t) = E\left(\frac{A}{A_S}\right)\varepsilon_T(t) \tag{1}$$

$$\dot{\varepsilon}(t) = -\frac{2C_0}{L}\varepsilon_R \tag{2}$$

$$\varepsilon(t) = \int_0^T \dot{\varepsilon}(t)dt \tag{3}$$

where *E*, *A* and C_0 are the Young's Modulus, the cross-section area and the elastic wave velocity of the bars, respectively; A_S and *L* are the cross-section area and the length of tested specimen, respectively. The data is valid only when the longitudinal stress in the specimen reaches the equilibrium state [47].

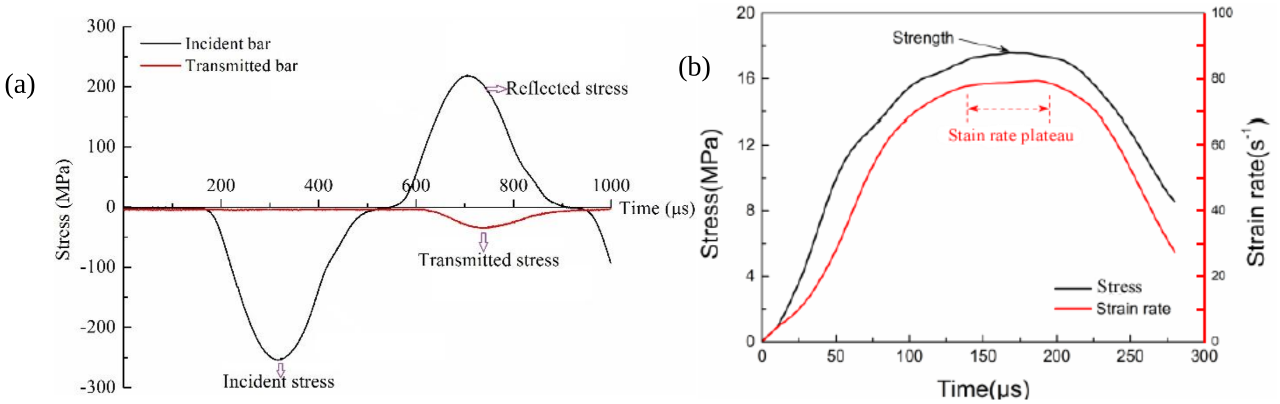

Fig. 5 Typical waves of SHPB tests (a) Measured signals, (b) Stress and strain rate time histories

Typical signals obtained from SHPB tests are illustrated in Fig. 5(a). Stress versus strain curves are derived from the voltage signals of the incident bar and the transmitted bar. According to Eq. (2), the strain rate is linearly correlated to the signal of the reflected wave. In general, the strain rates achieved in the SHPB test are not constant throughout the test. In this study, the reflected signal can almost reach a plateau with relatively constant values, as shown in Fig. 5(b). The strain rate at the ultimate strain (strain at peak stress) is taken as the representative strain rate in the SHPB tests and the peak value of the stress time history is regarded as the material strength. The achievement of stress equilibrium is essential for a valid SHPB test [47]. Eq. (4) is used to obtain the stress wave at the incident surface of the specimen in SHPB tests, which is compared with the transmitted stress wave to check the stress equilibrium. As shown in Fig.6, the time lags are removed for comparisons and the stress at the incident surface matches with the transmitted stress at peak values. It can be concluded that the stress equilibrium is achieved in this study.

$$\sigma_{IS} = \sigma_I + \sigma_R \tag{4}$$

where σ_{IS} denotes the stress at the incident surface of the specimen, σ_I and σ_R are the incident and reflected stresses, respectively.

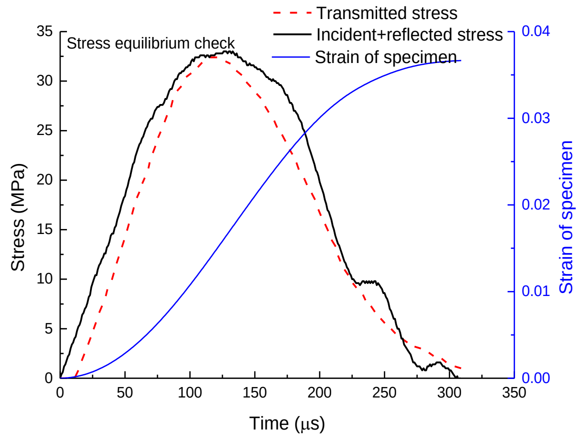

Fig.6 Stress equilibrium

4.3 Failure processes and modes

The failure patterns of RCC specimens with different dimensions at the strain rates of 30~80 /s after tests are observed and compared in Fig. 7. It is found that the size and number of generated fragments are directly related to the applied strain rate. The failure patterns are similar for two groups of specimens with different aggregate grades and similar for specimens with different sizes, indicating aggregate size and specimen size do not affect the failure modes of specimens in this strain rate range, but the failure modes strongly depend on the strain rate. As depicted in Fig. 7, the higher strain rate leads to more severe damage to the specimen. The failure mechanism can be explained through failure patterns, which can be classified into three categories, i.e. interfacial transition zones (ITZ) failure, crack cutting through aggregate, and aggregate fracture, as shown in Fig.8. The failure pattern of RCC changes with the increasing strain rate. Under low strain rate the specimens start cracking along the interfacial transition zones (ITZ) around the aggregates and specimens break into several large pieces without damaging the stronger aggregates (Fig.8 (a)). With increment in strain rates, the cracks propagate inside the specimen along the shortest paths cutting through the aggregates (Fig.8 (b)). When the strain rate further increases, the regions with coarse aggregates experience multiple cleaving instead of crack evolution through the weakest surface. A great portion of the cracks is accounted at higher strain rates so that the aggregate is fractured into small pieces (Fig.8(c)). It can be concluded that the sensitivity of failure mode of RCC materials to strain rate is similar to that of the traditional concrete [26].

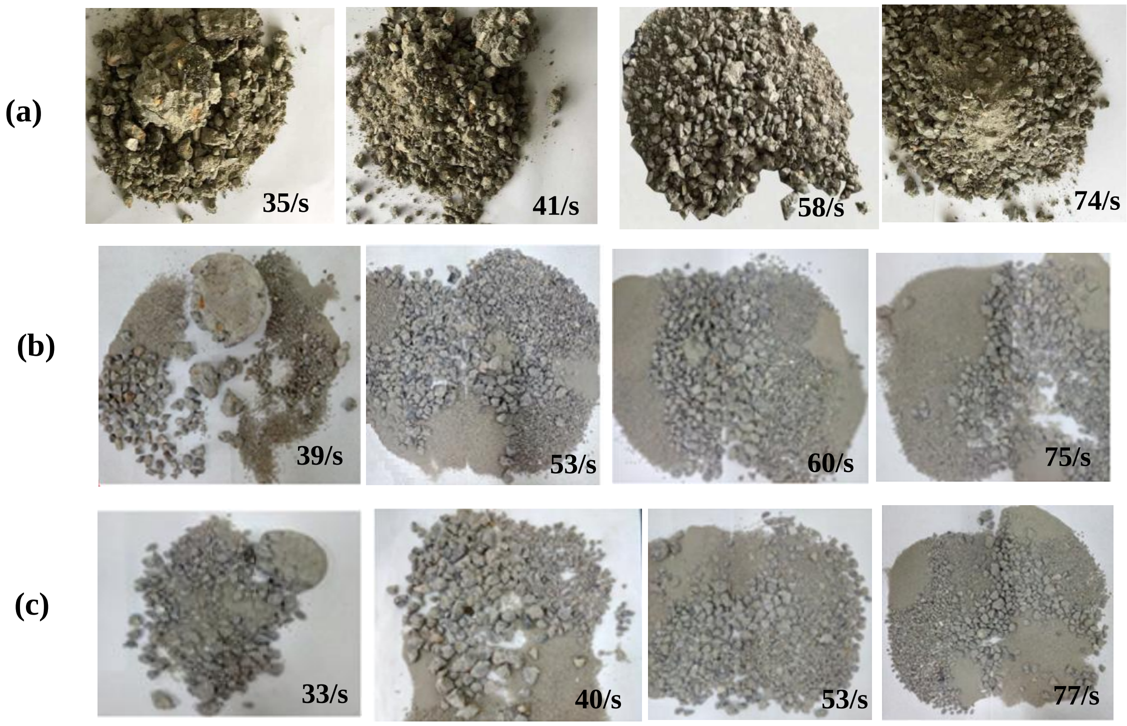

Fig.7 Failure patterns of RCC specimens with different specimen sizes under different strain rates. (a) Ø100-50mm specimens, (b) Ø75-37.5mm specimens, (c) Ø50-25mm specimens

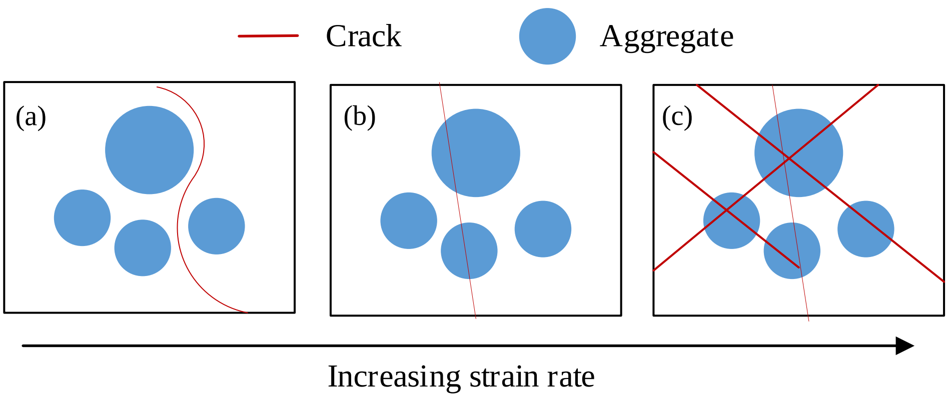

Fig.8 Schematic diagrams of failure patterns of RCC at different strain rates (a) Interfacial transition zones (ITZ) failure, (b) Crack cutting through aggregate, (c) Aggregate rupture

4.4 Stress–strain curves and energy absorption

As shown in Fig.9 and Fig.10, the typical stress–strain curves of different specimens under three strain rates in the range of 35/s~74/s are derived from the SHPB testing data. It is noted that the compressive strength of RCC materials is sensitive to strain rate, which is similar to the dynamic behavior of conventional concrete in the literatures [9, 26, 49]. As shown in Fig.9(c), the typical compressive strength of Ø100-50mm specimen at the strain rate of 65 /s is 21.37 MPa, which is approximately 1.85 times of the quasi-static strength. It is believed that viscous resistance of water content and the inertia effect contribute to delaying the creation and propagation of micro cracks, showing strain rate effect[50]. Increasing the diameter of the concrete specimens from 50 mm to 100 mm leads to dramatically rising in compressive strengths at high strain rate, as shown in Fig.9(a)~(c). The material behaves more obvious plasticity plateau at a higher strain rate, i.e. at the stain rate around 60 /s ~70 /s, which indicates that RCC material exhibits dynamic strengthening effect and better ductility with the rising strain rate. As shown in Fig.9 and Fig.10, the dynamic compressive strength of RCC specimens with finer aggregate grading Ⅰ is higher than that with aggregate grading Ⅱ under similar strain rate.

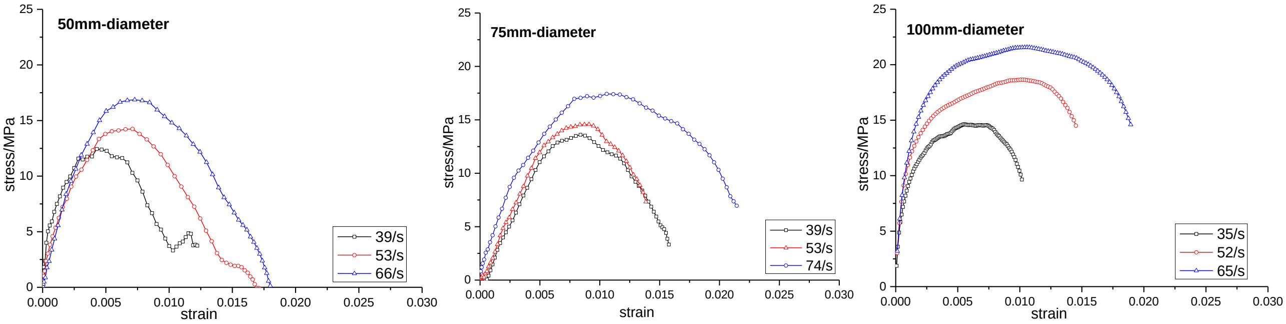

(a) (b) (c)

Fig.9 Typical stress-strain curves of RCC specimens with aggregate grading Ⅰ under different strain rates. (a) Ø50-25mm specimens, (b) Ø75-37.5mm specimens, (c) Ø100-50mm specimens

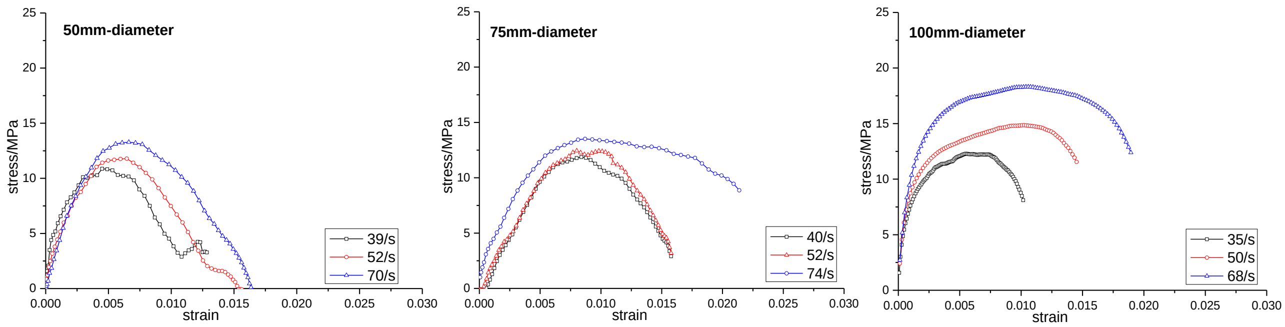

(a) (b) (c)

Fig.10 Typical stress-strain curves of RCC specimens with aggregate grading Ⅱ under different strain rates. (a)

Ø50-25mm specimens, (b) Ø75-37.5mm specimens, (c) Ø100-50mm specimens

In order to study the combined effect of ductility and strength of RCC material, energy absorption capability is calculated and it is defined as the specimen volume multiplied by the strain energy density (i.e. the area under the stress–strain curve) [51]. An integration has been performed to determine the strain energy density as given below

$$W = \int \sigma d\varepsilon \tag{5}$$

where W denotes the strain energy density, σ is the stress and ε represents strain. Table 3 summaries the compressive strength, the corresponding critical strain, dynamic increase factor of compressive strength obtained from experimental tests (DIF_{TOT}) and energy absorption properties of RCC specimens with two types of aggregate grading under different strain rates. The DIF obtained from experimental tests (DIF_{TOT}) is calculated by the dynamic compressive strength normalized by the corresponding quasi-static compressive strength as given in Table 3.

Table 3. Dynamic Mechanical Properties with Different Parameters

Specimen diameter (mm)	Aggregate grading	Typical specimen number	Strain rate (/s)	Average peak stress (MPa)	Average DIF_{TOT}	Average critical strain (%)	Average energy absorption W (kJ/m^3)
100	I	a1-1, a1-4, a1-7*	35	14.67	1.27	0.740	158.50
		f1-1, f1-3*,f1-4	52	18.71	1.62	1.077	260.60
		i1-1, i1-3*,i1-4	65	21.37	1.85	1.375	380.50
100	II	A1-1, A1-3*, A1-5	35	12.31	1.21	0.750	149.80
		F1-2, F1-3*, F1-6	50	14.85	1.46	1.051	220.46
		I1-1, I1-3*, I1-5	68	18.31	1.80	1.088	347.42
75	I	e1-1, e1-3*, e1-4	39	13.63	1.18	0.761	168.84
		g1-2, g1-3*, g1-4	53	14.55	1.26	0.910	227.10
		j1-2, j1-3*, j1-4	74	17.44	1.51	1.292	404.70
75	II	E1-1, E1-3*, E1-6	40	11.89	1.17	0.633	159.40
		G1-1, G1-4*, G1-5	52	12.41	1.22	0.793	210.20
		J1-1, J1-3*, J1-5	74	13.52	1.33	0.884	356.70
50	I	c1-1, c1-3*, c1-5	39	12.41	1.07	0.583	166.80
		d1-2, d1-4*,d1-5	53	14.21	1.23	0.891	281.60
		h1-2, h1-3*,h1-5	66	16.86	1.46	1.134	411.30
50	II	C1-1, C1-3*, C1-4	39	10.68	1.05	0.652	141.50
		D1-2, D1-4*, D1-5	52	11.80	1.16	1.051	278.30

Specimen diameter (mm)	Aggregate grading	Typical specimen number	Strain rate (/s)	Average peak stress (MPa)	Average DIF_{TOT}	Average critical strain (%)	Average energy absorption W (kJ/m^3)
		H1-1, H1-3*, H1-6	70	13.22	1.30	1.136	401.50

Note: *denotes the specimen with bedding surface. DIF_{TOT} is the compressive strength DIF obtained from experimental tests directly.

4.5 Dynamic Increase Factor

The DIF_{TOT} of the compressive strengths directly obtained from RCC experimental tests on different specimen sizes and aggregate grading are illustrated in Fig. 11. It is found that compressive strength of RCC is sensitive to strain rate, as well as the specimen size, indicating the structural effect associated with the lateral inertial confinement [21]. RCC is a kind of heterogeneous material with mortar matrix, aggregates, initial inherent micro-cracks, discontinuities and voids, which can propagate and fracture during loading. When subjected to a higher strain rate, cracks have no time to seek weak sections to propagate, but propagate through stronger aggregates as shown in Fig. 7, leading to the strength increment. At the same time the internal pore of the specimen is restrained due to viscosity effect of confined water and air in pores, which also leads to the increase of dynamic compressive strength. Therefore the directly obtained strength increment in experimental tests, DIF_{TOT}, consists of strain rate effects associated to the changing damage modes and viscosity effects of confined air and water in pores, and structural effect owing to lateral inertia confinement. The lateral inertia confinement is a structural effect, which does not reflect the true strain rate effect on material property, therefore should be removed in deriving the DIF for RCC from the experimental data [22]. Discussions on obtaining the true dynamic compressive strength and the corresponding empirical DIF formulae for RCC material are given in Section 5.1.

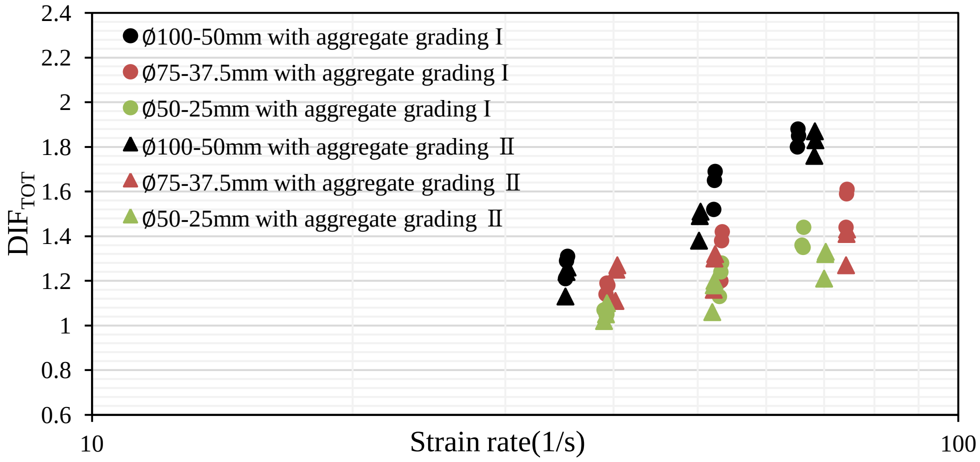

Fig.11 Comparison of DIF_{TOT} obtained from experimental tests with different RCC specimen sizes and aggregate grading

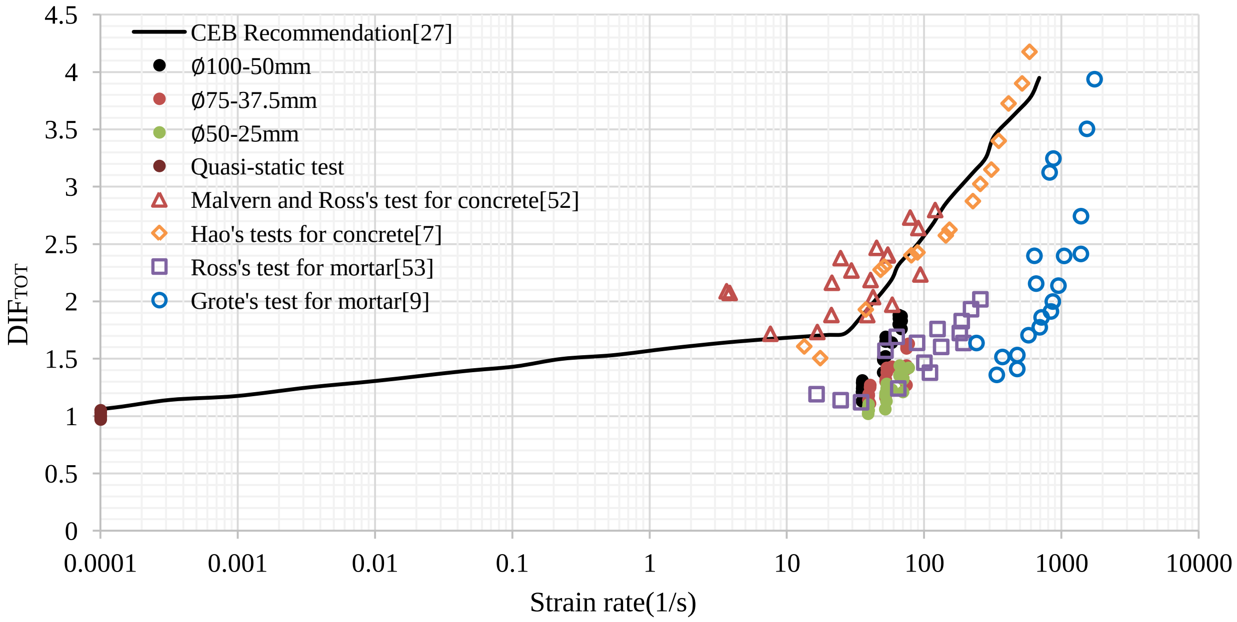

Fig.12 Experimental results compared with other testing results in [7, 9, 27, 52, 53]

The DIF_{TOT} based on experimental results of RCC are compared with some other testing results in [7, 9, 52, 53] and CEB recommendation [27] for traditional concrete as shown in Fig. 12. It can be found that the DIF_{TOT} of compressive strength for RCC material obtained from tests generally match the data from the the results from Ross's tests [53] for mortar in the strain rate range between 10 /s and 80 /s. In addition, the DIF_{TOT} values for RCC material are lower than that of conventional concrete from CEB recommendation [27], Malvern and Ross's tests [52] and Hao's test [7], which means RCC is less sensitive to strain rate than conventional concrete in terms of compressive strength. This is because RCC is drier than conventional concrete therefore less water viscosity effect.

5. Influencing factors on dynamic compressive properties

5.1 Lateral inertia confinement effect

The influence from lateral inertia confinement as a structural effect always exists in the high strain rate tests. The lateral inertia confinement is dependent on the density of the material and the size of the tested samples. Under high strain rate loading, the specimen inevitably undergoes lateral deformation due to the Poisson's effect. The lateral deformation results in inertia force as a confinement to limit its deformation. The specimens with different diameters, i.e. 50 mm, 75 mm and 100 mm, are prepared in this study for SHPB tests to examine the structural effect at high strain rate. The obtained DIF_{TOT} from laboratory tests of RCC with different diameters are shown in Fig.12 and Table 3. As can be seen, the DIF_{TOT} values increase with the specimen diameter due to the lateral inertia confinement effect. The findings are consistent with those by other researchers [54]. In addition, the difference of DIF_{TOT} values among specimens with different dimensions becomes more significant with the increasing strain rate, indicating the influence of lateral inertia confinement is also strain rate sensitive.

The material strength enhancement by using DIF_{TOT} directly obtained from laboratory tests will overestimate the true dynamic material strength. The previous research [21] as well as the testing data presented above have proved the contributions of lateral inertia confinement to DIF_{TOT}. Therefore, the lateral inertia confinement effects need to be removed to derive the true dynamic material strength at high strain rates [22]. In a previous study, numerical simulations were carried out to quantify the lateral inertia confinement effect on concrete strength increment with strain rate [21]. The same approach is adopted here. Numerical simulations of SHPB tests on RCC specimens at different strain rates are carried out by setting the material DIF as 1.0. Therefore, the numerically obtained strength increment of the material is attributed purely to lateral inertia confinement. The lateral inertia confinement effect contribution to DIF_{TOT} of RCC obtained from numerical simulations in this study for different sizes of specimens are shown in Fig13. It is shown that lateral inertia confinement effect on RCC specimens is dependent on specimen size as expected. Lateral inertia confinement contributions are about 4%~13%, 0%~5% and 0%~2% for Ø100-50mm, Ø75-37.5mm and Ø50-25mm, respectively, when the strain rate is in the rage of 10/s ~ 80 /s. True DIF of RCC, expressed as $DIF_{\dot{\varepsilon}}$, can be obtained from the test data by deducting the numerically obtained dynamic strength increment due to lateral inertia confinement [22]. The obtained $DIF_{\dot{\varepsilon}}$ and the best-fitted curve for the RCC are plotted in Fig. 14. As can be noted the obtained DIF values are specimen size independent after the lateral inertia confinement contribution to strength increment is removed. The empirical formulae of $DIF_{\dot{\varepsilon}}$ for RCC material in terms of compressive strength are derived as below

$$DIF_{\dot{\varepsilon}} = 0.02669(\log \dot{\varepsilon}) + 1.09872 \qquad for \qquad 0.0001/s < \dot{\varepsilon} \leq 30/s \tag{6}$$

$$DIF_{\dot{\varepsilon}} = 2.39591(\log \dot{\varepsilon})^2 - 7.09013(\log \dot{\varepsilon}) + 6.336 \qquad for \qquad 30/s < \dot{\varepsilon} \leq 80/s \tag{7}$$

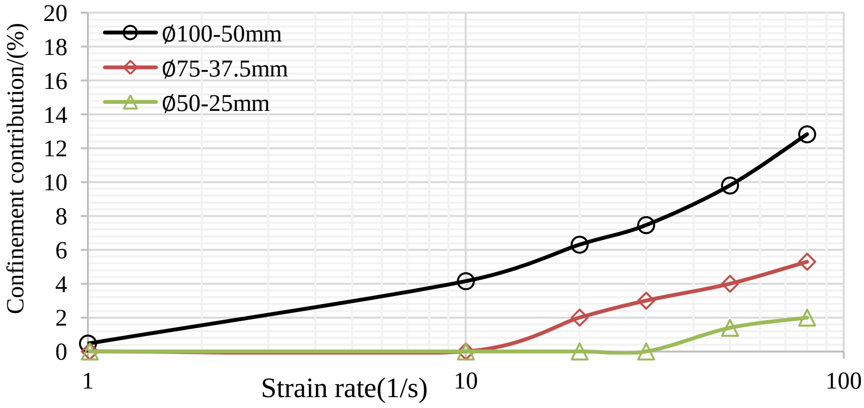

Fig.13 The contribution to DIF_{TOT} by lateral inertia confinement

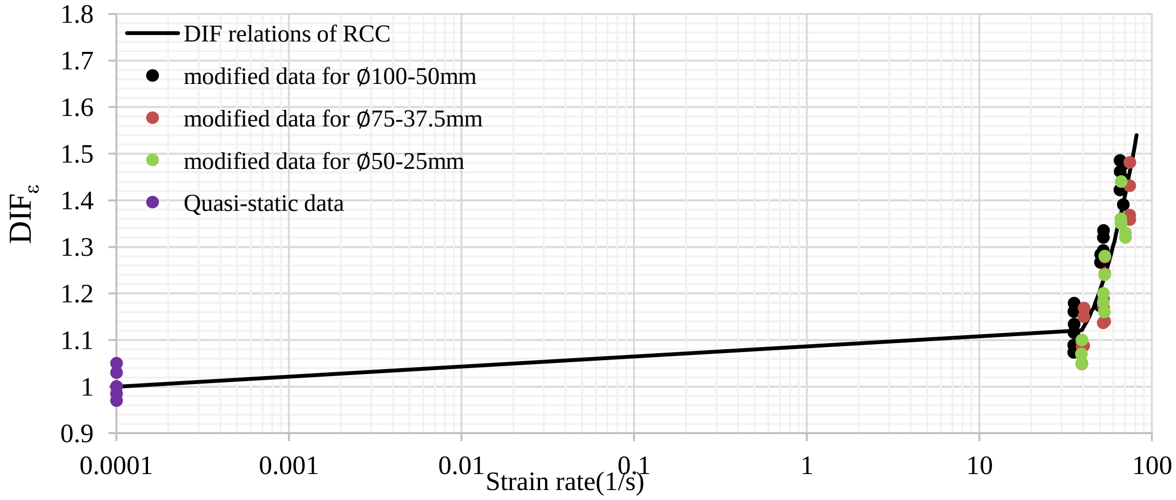

Fig.14 The true compressive strength $DIF_{\dot{\varepsilon}}$ of RCC material

5.2 Aggregate grading effect

The effects of aggregate size on the RCC compressive strength at high strain rate are also investigated. Fig.15 shows the stress–strain curves of RCC specimens of Ø75-37.5mm and Ø100-50mm with different aggregate grading. It can be observed that the peak stress and Young's modulus increase with the rising strain rate significantly and the RCC specimens show an obvious strain rate effect. Moreover, the curves with smaller aggregates (aggregate grading Ⅰ) are above the curves with larger aggregates (aggregate grading Ⅱ) at the similar strain rate, which means the compressive strength decreases with the increasing aggregate size. This is because more failure surfaces are generated by the existence of more number of smaller aggregates, which requires more energy to fracture the RCC specimens. After reaching the peak stress, the specimens enter softening phase. As shown in Fig. 15, the specimens with aggregate grading Ⅰ show more obvious softening than the specimens with aggregate grading Ⅱ.

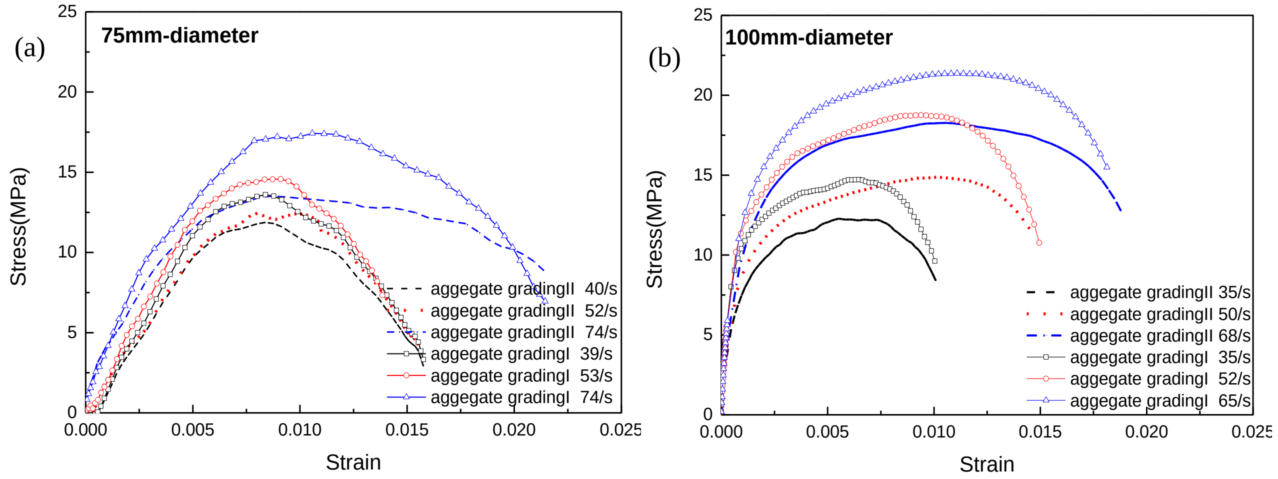

Fig.15 Stress–strain curves of RCC specimens with different aggregate grading. (a) Ø75-37.5mm specimens, (b) Ø100-50mm specimens

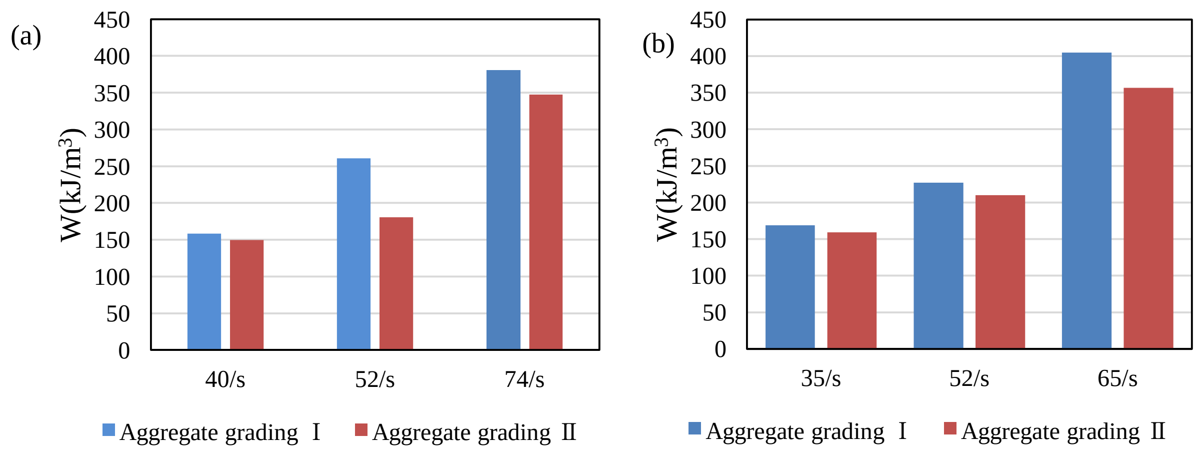

Fig.16 Specific energy absorption of RCC with different aggregate gradings (a) Ø75-37.5mm specimens, (b) Ø100-50mm specimens

Compressive strength DIF values of the specimens with different aggregate grading are listed in Table 3. The DIF_{TOT} of the specimens with aggregate grading Ⅰ are higher than those with aggregate grading Ⅱ. Because given the same volumes of aggregates in two batches of specimens, the specimens with larger aggregates have fewer numbers of aggregates, which leads to less cleaving surfaces under the same strain rate. In addition, due to the increasing heterogeneity caused by the larger coarse aggregates in the specimen, the obtained DIF_{TOT} are more dispersive than those of the specimens with smaller aggregates. These results indicate that roller compacted concrete mixed with smaller size aggregate perform better under dynamic loadings, which is similar to the conclusion drawn by Hao et al [7]. As shown in Fig.16, the specific energy absorption capacities of RCC material under the strain rates between 35 /s ~ 74 /s are compared. It is found that the specimens with aggregate grading Ⅰ can absorb more energy than the specimen with aggregate grading Ⅱ for both Ø75-37.5mm specimens and Ø100-50mm specimens. The specimens with aggregate grading Ⅰ can absorb more energy to fracture into more small pieces. The enhancement of energy absorption becomes more prominent with the increasing strain rate. For instance, the energy absorption of the specimens with aggregate grading Ⅰ at the strain rate of 74 /s is 380 kJ/m^3, which is significantly higher than 260 kJ/m^3 at the strain rate of 52 /s and 155 kJ/m^3 at the strain rate of 40 /s.

5.3 Bedding surface effect

In the past, less attention was paid to the bedding surface between layers of RCC material. However, the influence of the bedding surface on structural performance is notable[55]. Based on the experimental and theoretical studies, the gradual change of Young's modulus and viscosity coefficient of the bedding surfaces for RCC dam has been studied in literature[40]. However, the study on the dynamic compressive properties of RCC affected by bedding surface is limited. In this study, the experimental results of RCC specimens with or without bedding surface under dynamic compressive loading are discussed. As mentioned above, among a total of 54 specimens, 18 of them have bedding surface, including 6 Ø100-50mm specimens, 6 Ø75-37.5mm specimens and 6 Ø50-25mm specimens. Fig. 17 shows the typical stress-strain curves of Ø100-50mm RCC specimens with and without bedding surface for aggregate grading Ⅰ and aggregate grading Ⅱ, respectively. It can be found that the trends of the curves of RCC specimens with and without bedding surface are similar. As expected, the specimen without bedding surface has slightly higher strength than the specimen with bedding surface at the similar strain rate. For example, the specimen of aggregate grading Ⅰ without bedding surface has the strength of 21.57 MPa at 65 /s and the specimen with bedding surface has the strength of 20.79 MPa at 65 /s. The specimen of aggregate grading Ⅱ without bedding surface has the strength of 18.61 MPa at 68 /s and the specimen with bedding surface has the strength of 17.90 MPa at 68 /s. The differences are minimum. Similarly it can be observed that the existence of bedding surface has insignificant influences on the Young's modulus of the specimen. This is because the bedding surface is very thin in the specimen. Its influence on both the specimen strength and stiffness is therefore negligible. Fig.18 shows the DIF_{TOT} values of the strength from RCC experimental tests with or without bedding surface under different strain rates and different aggregate grading. As shown, the RCC specimen without bedding surface has slightly higher DIF_{TOT} of compressive strength than the specimen with bedding surface at the strain rate between10 /s ~ 80 /s. However, the influence of the bedding surface is insignificant therefore in the above analysis the data obtained from specimens with or without bedding surface are used together in deriving the dynamic strength increment of RCC with strain rate.

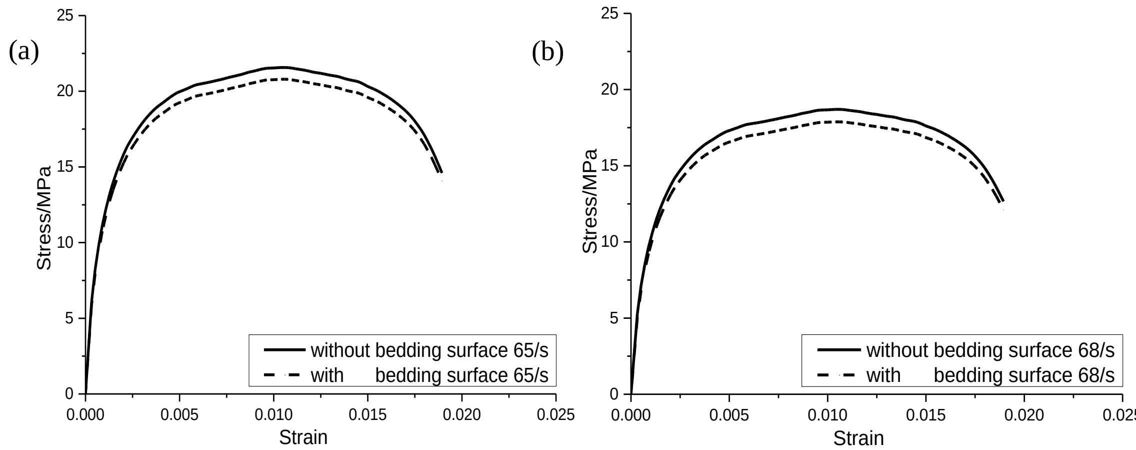

Fig.17 The effect of bedding surface on typical stress-strain curves of Ø100-50mm specimens (a) Specimens with aggregate grading Ⅰ, (b) Specimens with aggregate grading Ⅱ

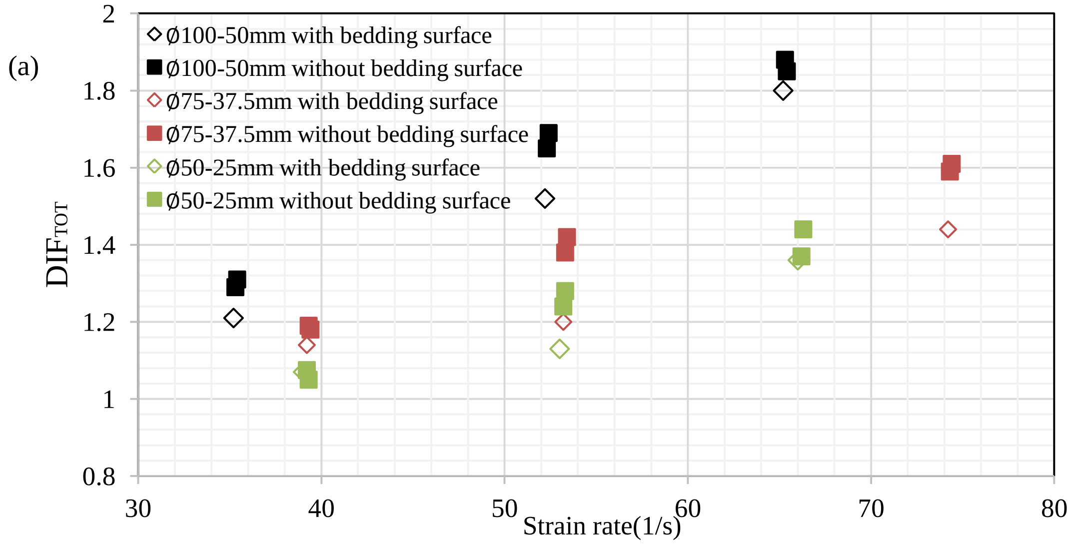

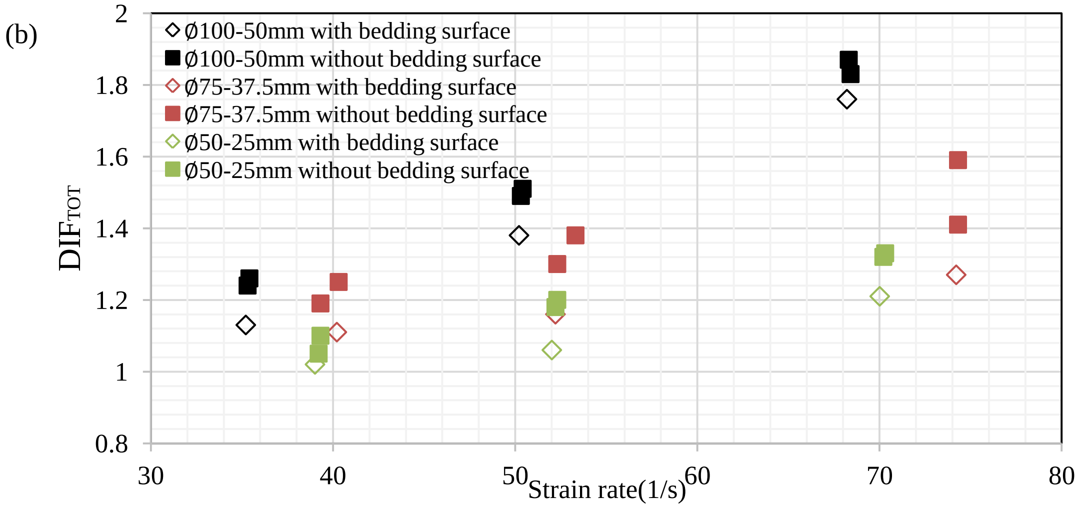

Fig.18 Comparision of DIF_{TOT} values obtained from RCC experimental tests with or without bedding surface. (a) Specimens with aggregate grading Ⅰ, (b) Specimens with aggregate grading Ⅱ

6. Conclusions

This study presents dynamic compressive properties of RCC by using Split Hopkinson Pressure Bar (SHPB). Three kinds of RCC specimens with the same L/D ratio (i.e. specimen length to diameter) of 0.5, but different diameters, i.e. 50 mm, 75 mm and 100 mm are prepared and tested under the strain rate up to 80 /s. The failure modes and stress–strain curves of the RCC material are captured and compared. It is found that RCC material is sensitive to strain rate. However, its sensitivity to strain rate is less significant as compared to normal concrete because RCC is drier and rolling compact probably also reduces the porous ratio of concrete. The effects of specimen size, aggregate grading and the existence of bedding surface of RCC on the dynamic compressive behavior are also discussed in this study. It is found that the dynamic compressive strength of RCC directly obtained from testing is specimen size dependent owing to lateral inertia confinement effect. The compressive strength of RCC decreases with the increasing aggregate size. With the existence of a thin bedding surface has minimum effect on RCC material properties. Based on the testing data, empirical formulae of true compressive strength DIF of RCC are proposed.

Acknowledgements

This research is supported by the National Natural Science Foundation of China (No.51509182), the Foundation for Innovative Research Groups of the National Natural Science Foundation of China (No.51321065) and Australian Research Council.

References

[1] K. Fang, Y. Ruan, L. Zeng, Late-age properties of RCC with low cement content and high fly ash content, Hydroelectr. Eng 67 (1999) 18-25.

[2] C.D. Atiş, Strength properties of high-volume fly ash roller compacted and workable concrete, and influence of curing condition, Cement and Concrete research 35(6) (2005) 1112-1121.

[3] M. Chi, R. Huang, Effect of circulating fluidized bed combustion ash on the properties of roller compacted concrete, Cement and Concrete Composites 45 (2014) 148-156.

[4] M. Rao, H. Yang, Y. Lin, J. Li, Y. Shi, Influence of maximum aggregate sizes on the performance of RCC, Construction and Building Materials 115 (2016) 42-47.

[5] D. Liu, Z. Li, J. Liu, Experimental study on real-time control of roller compacted concrete dam compaction quality using unit compaction energy indices, Construction and Building Materials 96 (2015) 567-575.

[6] A. Lopez-Uceda, F. Agrela, M. Cabrera, J. Ayuso, M. López, Mechanical performance of roller compacted concrete with recycled concrete aggregates, Road Materials and Pavement Design (2016) 1-20.

[7] Y. Hao, H. Hao, G. Jiang, Y. Zhou, Experimental confirmation of some factors influencing dynamic concrete compressive strengths in high-speed impact tests, Cement and concrete research 52 (2013) 63-70.

[8] X. Zhou, H. Hao, Modelling of compressive behaviour of concrete-like materials at high strain rate, International Journal of Solids and Structures 45(17) (2008) 4648-4661.

[9] D. Grote, S. Park, M. Zhou, Dynamic behavior of concrete at high strain rates and pressures: I. experimental characterization, International Journal of Impact Engineering 25(9) (2001) 869-886.

[10] S. Park, Q. Xia, M. Zhou, Dynamic behavior of concrete at high strain rates and pressures: II. Numerical simulation, International journal of impact engineering 25(9) (2001) 887-910.

[11] M. Zhang, H. Wu, Q. Li, F. Huang, Further investigation on the dynamic compressive strength enhancement of concrete-like materials based on split Hopkinson pressure bar tests. Part I: Experiments, International journal of impact

engineering 36(12) (2009) 1327-1334.
[12] D. Zheng, Q. Li, An explanation for rate effect of concrete strength based on fracture toughness including free water viscosity, Engineering Fracture Mechanics 71(16) (2004) 2319-2327.
[13] P. Rossi, A physical phenomenon which can explain the mechanical behaviour of concrete under high strain rates, Materials and Structures 24(6) (1991) 422-424.
[14] J. Eibl, B. Schmidt-Hurtienne, Strain-rate-sensitive constitutive law for concrete, Journal of Engineering Mechanics 125(12) (1999) 1411-1420.
[15] P. Bischoff, S. Perry, Compressive behaviour of concrete at high strain rates, Materials and structures 24(6) (1991) 425-450.
[16] C.A. Ross, J.W. Tedesco, S.T. Kuennen, Effects of strain rate on concrete strength, Materials Journal 92(1) (1995) 37-47.
[17] H. Aoyama, H. Noguchi, Mechanical Properties of Steel and Concrete Under Load Cycles Idealizing Seismic Actions, AICAP-CEB Symposium on Structural Concrete under Seismic Actions, 1979, pp. 25-28.
[18] P. Rossi, Influence of cracking in the presence of free water on the mechanical behaviour of concrete, Magazine of concrete research 43(154) (1991) 53-57.
[19] P. Rossi, J.G. van Mier, C. Boulay, F. Le Maou, The dynamic behaviour of concrete: influence of free water, Materials and Structures 25(9) (1992) 509-514.
[20] D. Yan, G. Lin, Influence of initial static stress on the dynamic properties of concrete, Cement and Concrete Composites 30(4) (2008) 327-333.
[21] Y. Hao, H. Hao, Z.-X. Li, Numerical analysis of lateral inertial confinement effects on impact test of concrete compressive material properties, International Journal of Protective Structures 1(1) (2010) 145-167.
[22] Y. Hao, H. Hao, Numerical evaluation of the influence of aggregates on concrete compressive strength at high strain rate, International Journal of Protective Structures 2(2) (2011) 177-206.
[23] Y. Hao, H. Hao, Finite element modelling of mesoscale concrete material in dynamic splitting test, Advances in Structural Engineering 19(6) (2016) 1027-1039.
[24] D. Yan, G. Lin, Dynamic properties of concrete in direct tension, Cement and concrete research 36(7) (2006) 1371-1378.
[25] H. Hao, Y. Hao, J. Li, W. Chen, Review of the current practices in blast-resistant analysis and design of concrete structures, Advances in Structural Engineering 19(8) (2016) 1193-1223.
[26] X. Chen, S. Wu, J. Zhou, Experimental and modeling study of dynamic mechanical properties of cement paste, mortar and concrete, Construction and Building Materials 47 (2013) 419-430.
[27] C.E.I. du Beton, CEB-FIP model code 1990, Bulletin d'Information 213 (1993) 214.
[28] C. Ross, Strain-rate-dependent constitutive equations for concrete, Journal of pressure vessel technology, transactions of the ASME 120 (1998) 398-405.
[29] M. Katayama, M. Itoh, S. Tamura, M. Beppu, T. Ohno, Numerical analysis method for the RC and geological structures subjected to extreme loading by energetic materials, International Journal of Impact Engineering 34(9) (2007) 1546-1561.
[30] Y. Hao, H. Hao, Influence of the concrete DIF model on the numerical predictions of RC wall responses to blast loadings, Engineering Structures 73 (2014) 24-38.
[31] C. Zhai, L. Chen, Q. Fang, W. Chen, X. Jiang, Experimental study of strain rate effects on normal weight concrete after exposure to elevated temperature, Mater. Struct. 50(1) (2017) 40.
[32] H. Zhao, A study on testing techniques for concrete-like materials under compressive impact loading, Cement and Concrete Composites 20(4) (1998) 293-299.
[33] Y. Tai, Uniaxial compression tests at various loading rates for reactive powder concrete, Theoretical and Applied Fracture Mechanics 52(1) (2009) 14-21.

[34] J. Xiao, L. Li, L. Shen, C.S. Poon, Compressive behaviour of recycled aggregate concrete under impact loading, Cement and Concrete Research 71 (2015) 46-55.

[35] Q. Li, F. Zhang, W. Zhang, L. Yang, Fracture and tension properties of roller compacted concrete cores in uniaxial tension, Journal of materials in civil engineering 14(5) (2002) 366-373.

[36] C. Atiş, U. Sevim, F. Özcan, C. Bilim, O. Karahan, A. Tanrikulu, A. Ekşi, Strength properties of roller compacted concrete containing a non-standard high calcium fly ash, Materials Letters 58(9) (2004) 1446-1450.

[37] A. Mardani-Aghabaglou, K. Ramyar, Mechanical properties of high-volume fly ash roller compacted concrete designed by maximum density method, Construction and Building Materials 38 (2013) 356-364.

[38] C. Zhang, G. Wang, S. Wang, Y. Dong, Experimental tests of rolled compacted concrete and nonlinear fracture analysis of rolled compacted concrete dams, Journal of materials in civil engineering 14(2) (2002) 108-115.

[39] H. Wang, W. Wen, Dynamic mechanical properties of RCC under uniaxial stress, Journal of Hydroelectric Engineering 4(5) (2011) 129-134.

[40] C. Gu, J. Song, H. Fang, Analysis model on gradual change principle of effect zones of layer face for rolled control concrete dam, Applied Mathematics and Mechanics 27(11) (2006) 1523-1529.

[41] C. Gu, L. Cheng, T. Li, Study on thin| layer element and application in FEM analysis of RCCD dams [J], Chinese Journal of Computational Mechanics 6 (2004) 015.

[42] G. Liu, J. Hao, Simplified numerical method in stress analysis of RCC arch dam with layered structure [J], Journal of Tsinghua University (Science and Technology) 1 (1996) 004.

[43] S. Wang, M. Zhang, S.T. Quek, Effect of specimen size on static strength and dynamic increase factor of high-strength concrete from SHPB test, Journal of Testing and Evaluation 39(5) (2011) 1-10.

[44] Y. Hao, H. Hao, Dynamic compressive behaviour of spiral steel fibre reinforced concrete in split Hopkinson pressure bar tests, Construction and Building Materials 48 (2013) 521-532.

[45] T. Lok, X. Li, D. Liu, P. Zhao, Testing and response of large diameter brittle materials subjected to high strain rate, Journal of Materials in Civil Engineering 14(3) (2002) 262-269.

[46] Y. Hao, H. Hao, Z. Li, Influence of end friction confinement on impact tests of concrete material at high strain rate, International journal of impact engineering 60 (2013) 82-106.

[47] Y. Lu, Q. Li, Appraisal of pulse-shaping technique in split Hopkinson pressure bar tests for brittle materials, International Journal of Protective Structures 1(3) (2010) 363-390.

[48] U. Lindholm, Some experiments with the split hopkinson pressure bar, Journal of the Mechanics and Physics of Solids 12(5) (1964) 317-335.

[49] Y. Lu, X. Chen, X. Teng, S. Zhang, Dynamic compressive behavior of recycled aggregate concrete based on split Hopkinson pressure bar tests, Latin American Journal of Solids and Structures 11(1) (2014) 131-141.

[50] J. Cui, H. Hao, Y. Shi, Discussion on the suitability of concrete constitutive models for high-rate response predictions of RC structures, International Journal of Impact Engineering (2017).

[51] J.B. Mander, M.J. Priestley, R. Park, Theoretical stress-strain model for confined concrete, Journal of structural engineering 114(8) (1988) 1804-1826.

[52] L.E. Malvern, D.A. Jenkins, T. Tang, C.A. Ross, Dynamic compressive testing of concrete, Proceedings of 2nd symposium on the interaction of non-nuclear munitions with structures. Florida, USA, 1985, pp. 194-199.

[53] C.A. Ross, J. Tedesco, Split-Hopkinson pressure-bar tests on concrete and mortar in tension and compression, Materials Journal 86(5) (1989) 475-481.

[54] Q. Li, H. Meng, About the dynamic strength enhancement of concrete-like materials in a split Hopkinson pressure bar test, International Journal of solids and structures 40(2) (2003) 343-360.

[55] Z. Wu, Safety monitoring theory & its application of hydraulic structures, Beijing: Higher Education (2003).